LANGMUIR

Article

Silica supported nitrogen-enriched porous benzimidazole-linked and triazine based polymers for the adsorption of CO2

Moorthy Maruthapandi, Lakshmanan Eswaran, Reut Cohen, Nina Perkas, John H. T. Luong, and Aharon Gedanken

Langmuir, **Just Accepted Manuscript** • DOI: 10.1021/acs.langmuir.0c00230 • Publication Date (Web): 09 Apr 2020

Just Accepted

is published by the American Chemical Society. 1155 Sixteenth Street N.W., Washington, DC 20036

Silica supported nitrogen-enriched porous benzimidazole-linked and triazine based polymers for the adsorption of CO_2

*Moorthy Maruthapandi[1], Lakshmanan Eswaran[1], Reut Cohen [1], Nina Perkas[1], John H. T. Luong[2], Aharon Gedanken[1]**

[1]Bar-Ilan Institute of Nanotechnology and Advanced Materials, Department of Chemistry, Bar-Ilan University, Ramat-Gan 52900, Israel.

[2]School of Chemistry, University College Cork, Ireland

* Corresponding authors: gedanken@mail.biu.ac.il, Fax: +972-3-7384053; Tel: +972-3-5318315

ABSTRACT

Two crystalline and five amorphous benzimidazole polymers (BINP) were synthesized and conjugated to porous silica via amine and aldehyde-based materials by a simple reflux procedure. The resulting polymers were subject to thermal analysis for monitoring and quantification of the adsorption and desorption of CO_2. All the polymers were capable of adsorbing CO_2 from a flowing stream of only 80 mL/min at 25 ^oC. The adsorbed CO_2 onto the polymers were effectively desorbed at room temperature, illustrating the potential application of such polymers for repeated adsorption/desorption of CO_2. The CO_2 adsorption capacities of these polymers were dependent upon their nitrogen content, specific surface area, and pore size. The available nitrogen atoms for binding to the carbon of CO_2 via tetrel bonds also plays an important role in the capture of this gas. Minimal and much lower CO_2 adsorption was also noted with two crystalline polymers, compared to the five amorphous counterparts. Intermolecular hydrogen bonding and π-π interaction effectively prevented the polymer N sites of the crystalline polymers from interacting with polarized CO_2 molecules.

Keywords; silica-based porous benzimidazole polymer, nitrogen-rich triazine polymer, CO_2 adsorption, desorption, mechanism study

Introduction

The greenhouse effect by CO_2, CH_4, and N_2O has become a serious issue over the past 20 years.[1-2] Among them, CO_2 contributes to 60% to the global warming due to its enormous emission amount from the utilization of carbon-based fuels. The quantity of CO_2 in the atmosphere is almost 404 ppm, which is pointedly over the preindustrial value of 280 ppm.[3-4] Some climate skeptics also claim that an increase of 45 percent is mainly caused by humans and their associated activities. Several adsorbents are used to adsorb or capture the CO_2, followed by the release of this gas, enabling the reuse of the adsorbents.[5–8] Two types of materials can be distinguished in terms of the CO_2 adsorption: i) solid adsorbents and ii) liquid adsorbents. Albeit the liquid adsorbents including popular monoethanolamine are the most convenient and simple method, the operation requires a large adsorbent volume and suffers from a high corrosion rate. Intensive energy is also needed to recover and regenerate the large quantities of water and liquid adsorbents as the heat treatment must be performed at >100 °C to release the chemically adsorbed CO_2. Organic or organic-inorganic mesoporous or microporous based materials are used to overcome these shortcomings and the key appealing feature is their significant energy saving.[9,10] Inorganic based materials are silica-coated polyaziridine, zeolites, inorganic capillary membranes, iridium based complex, silica, etc.[10–12] Porous organic-based materials with different functional groups include microporous carbons, metal-organic frameworks (MOFs), porous organic molecules, and covalent organic polymers.[13,14] These organic materials exhibit desirable properties such as high surface area, thermal stability, chemical stability, facile synthesis, lightweight and diverse availability. [3,15–

[17] The amine groups are playing major in the adsorption of CO_2 via the binding or interaction between the amine and CO_2.[18, 19]

This study describes the synthesis of amorphous and crystalline nitrogen-enriched porous benzimidazole-linked polymers with conjugated imine functional groups. Such nitrogen-enriched porous benzimidazole-linked polymers are conjugated to porous silica to enable the use of thermogravimetric analysis (TGA) for probing the adsorption and desorption of CO_2 at ambient temperature. A systematic study is then conducted to investigate the adsorption capacity of these polymers for CO_2 with respect to their surface area, pore size, nitrogen content, and crystallinity. The rationale behind the adsorption/desorption of CO_2 by the silica-based polymers is proposed in corroboration with the experimental data.

Materials and methods

Chemicals

4-Aminophenyl sulfone, 4,4-oxydianiline, 1,2,4,5-benzenetetramine tetrahydrochloride, tris(4-formylphenyl)amine, dimethylformamide (DMF), 4,4-diaminodiphenylmethane, 4-(4-formylphenoxy)benzaldehyde, melamine, and tetraethyl orthosilicate.

Preparation of SiO_2

Deionized water (10 mL) containing 1 g of tetraethyl orthosilicate was added to 90 mL of ethanol in a 100 mL beaker. The reaction mixture was sonicated 5 min until the temperature reaches 60 °C. Ammonium hydroxide (28 %, 2 mL) was added to the reaction mixture to control pH 8–9. The clear solution turned white turbid and sonicated for 40 min in a sonicated cell placed in an ice bath. The solid product was filtered and washed several times with deionized water, followed by vacuum drying.

Synthesis of amine functionalized silica (A-f-Si)

SiO_2 (0.5 g) and 1.2 mL of (3-aminopropyl) triethoxysilane were added to 50 mL of toluene in a 100 mL- round bottom flask. The reaction mixture was refluxed in an oil bath for 24 h at 120 ^oC under the N_2 atmosphere. The product (designated as A-f-Si) was filtered, washed several times with ethanol, and vacuum dried.

Synthesis of benzimidazole-linked polymers

BINP-1 polymer. A-f-Si (0.15 g) and 0.5 g of tris(4-formylphenyl) amine were added to 30 mL of DMF in a 100 mL three-necked flask. After refluxing at 90 ^oC for 45 min, 0.6 g of 1,2,4,5-benzenetetramine tetrahydrochloride was added and the reflux was continued at 180 ^oC for 24 h under the N_2 atmosphere. The final product was washed with methanol and vacuum dried. Similarly, other BINP polymers were synthesized using the same procedure with pertinent chemicals unless otherwise stated.

BINP-2 polymer. 0.35 g of 4-(4-formylphenoxy) benzaldehyde, 25 mL of DMF and 0.6 g of 1,2,4,5-benzenetetramine tetra hydrochloride.

BINP-3 polymer. 0.35 g of tris(4-formylphenyl) amine and 0.3 g melamine.

BINP-4 polymer. 0.5 g of 4-(4-formylphenoxy) benzaldehyde and 0.4 g melamine.

BINP-5 polymer. 0.5 g of 4-(4-formylphenoxy) benzaldehyde and 0.4 g 4,4-oxydianiline.

BINP-6 polymer. 0.5 g of 4-(4-formylphenoxy) benzaldehyde and 0.5 g 4-aminophenyl sulfone.

BINP-7 polymer. 0.35 g of 4-(4-formylphenoxy) benzaldehyde and 0.4 g 4,4-diaminodiphenyl methane.

Instrumentation and procedure for the CO_2 capture

Thermogravimetric analysis (TGA) was performed with the PerkinElmer 'Pyris 1' TGA instrument. The TGA instrument is equipped with the additional built-in gas inlet to switch the nitrogen gas to the CO_2 gas and vice versa. [9,11] Each polymer (~5-11 mg) was placed in an alumina crucible before the analysis in the TGA oven. The materials were dried at 105 °C with a heating rate of 40 °C/min under the N_2 atmosphere, followed by nitrogen-purging for 20 min. The system was cooled to 20 °C at 40°C /min and kept at 20 °C for 10 min. For the capture of CO_2, the flowing gas was switched to CO_2 and hold under the gas pressure for 40 min. For the desorption process, the gas was switched again to nitrogen and hold at 20 °C for 40 min. The CO_2 capture was analyzed by the weight increase of the sample upon switching from N_2 to CO_2. Once the CO_2 capture on the samples approached equilibrium, the gas was switched back to N_2 for the desorption of CO_2. These steps were repeated 3 times (balance purge 80 mL/min; sample purge 20 mL/min). The chemical structures of the BINP polymers are shown in Scheme 1.

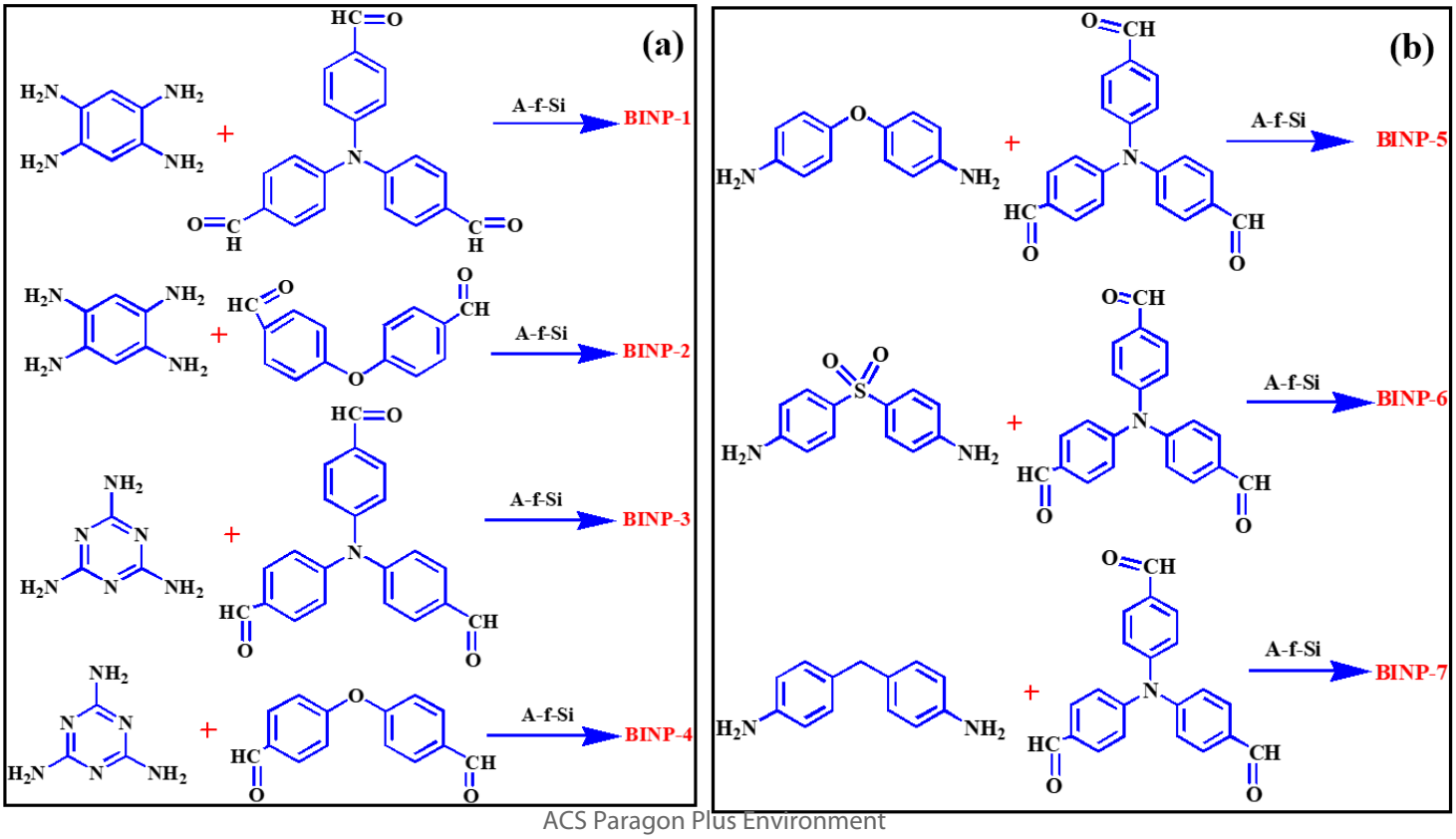

Scheme 1. (a) and (b), the chemical reactions of all seven BINP polymers

Analysis

FTIR spectra were acquired by a Transon 27 instrument, from Bruker Inc. (Germany), equipped with a diamond tip. The polymer morphology was probed by high resolution scanning electron microscopy (HRSEM) using an FEI Megallon 400 L microscope. The polymers for HRSEM were prepared by placing a small amount of the dried powder on a carbon tape attached to a copper plate, followed by sputtering a thin gold film coating on top of the powder (working distance is 6-7.1 mm and accelerating voltage is 5 kV). The solid-state properties of the synthesized polymer materials were recorded using a Bruker Inc. (Germany) AXS D8 Advance diffractometer with a reflection of θ-geometry, 40 kV and 30 mA using Cu Kα (λ=1.5418 Å) as the radiation source, with a receiving slit of 0.2 mm and a high-resolution energy-dispersive detector. All MAS NMR measurements were conducted on a Bruker Advance III 5000 MHz narrow-bore spectrometer, using a 4 mm double-resonance MAS probe. ^{13}C CPMAS was carried out at a spinning rate of 8 kHz, using a 2.5 μs 1H 90^{o} pulse, 2 ms mixing time and a 3 s recycle delay between acquisitions. NMR spectra were acquired using a Bruker 5000 Ultra Shield spectrometer with 400 MHz NMR (Bruker, Billerica, MA, USA). Thermal properties of the polymers were conducted by a thermogravimetric analyzer (model Pyris 1, TGA, Perkin Elmer). The BET measurements for the specific surface area, pore volume, and pore size distribution were measured using a Nova 3200e Quantachrome analyzer. Before analysis, the samples were subjected to heating at 120 ^{o}C under vacuum for 2 h. The surface area was calculated from the linear part of the BET plot. The pore size distribution was estimated using the Barrett–Joyner–Halenda (BJH) model and the Halsey

equation whereas the pore volume was measured at the P/P_0 0.9947 signal point. X-ray photoelectron spectroscopy (XPS) analysis was carried out using a Nexsa spectrometer (England) equipped with a monochromatic, micro-focused, low power Al Ka X-ray source (photon energy 1486.6 eV). Survey and high-resolution spectra were acquired at pass energy of 200 eV and 50 eV, respectively. Source power was normally 72W. The binding energies of all of the elements were recalibrated by setting the CC/CH component of the C 1s peak at 285 eV unless otherwise specified. Quantitative surface chemical analysis was performed using high-resolution core-level spectra after the removal of a nonlinear Smart background. The measurements were performed under UHV conditions, at a base pressure of $9.9x10^{-10}$ mBar (and no higher than $1.0x10^{-7}$ mBar). The spectra obtained were analyzed and deconvoluted using Advantage Software. Overlapping signals were analyzed after the deconvolution into Gaussian/Lorentzian-shaped components

Result and discussion

FT-IR analysis

A broad peak around 3500-3000 cm^{-1} of the benzimidazole polymers confirmed the polymerization of benzimidazole (Figure 2a), in agreement with the literature report. The sharp peaks at 3383, 3060, 1585, and 1455 cm^{-1} were attributed to the symmetrical and asymmetrical amine (N-H) stretching vibrations. The peaks between 1400 and 1600 cm^{-1} were assigned to C=C aromatic stretching vibrations. The peaks at 2915 and 2851 cm^{-1} represented the C-H aromatic stretching vibration and the peaks at 1585 and 1533 cm^{-1} were ascribed to the C=C stretching vibration. The stretching vibration peak at 1318 cm^{-1} was attributed to the C-N functional group. The peak at 822 cm^{-1} represented the out-of-plane bending vibration of amine.[20–22] The N=C peak at 1608 cm^{-1} was assigned to the vibration of the benzimidazole linkage. The intensity of 1698 cm-^{1} carbonyl stretching vibration was significantly attenuated in the BINP polymers, suggesting the complete

formation of the polymers. All significant IR peaks and the corresponding functional groups are given in Table 1.

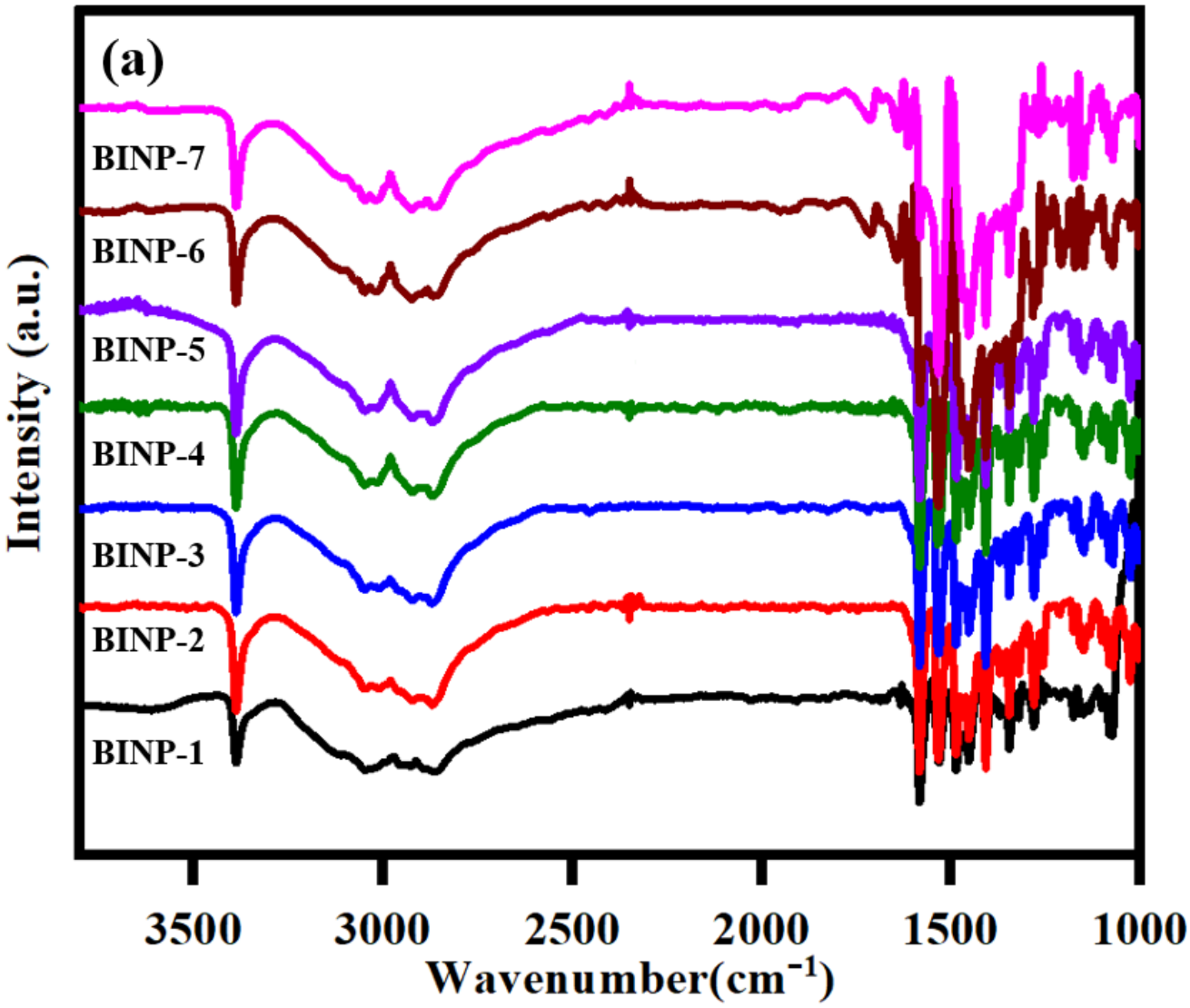

Figure 1. a) FTIR-spectra of the synthesized BINP polymers.

Table 1: The peaks in the IR absorption frequency region of benzimidazole polymers and its functional groups

BINP-Polymers Absorption frequency (cm^{-1})	Major functional groups
3383 3060 1455 1283	N-H (symmetrical and asymmetrical stretching vibration)
1400, 1600	C=C (aromatic stretching vibration)
2901, 2851	C-H (stretching vibration)
1318	C=C (stretching vibration)
824	out-of-plane bending vibration mode of N-H
1608	N=C- imine stretching vibration

XRD analysis

The broad diffraction peaks of BINP-1 to BINP-5 were almost identical as shown in Figure 2. Each XRD spectrum includes a broad peak around $2\theta = 15.4^{o}$- 32.9^{o}, representing the repeated units of benzimidazole linkage. The sharp diffraction peaks of BINP6 and BINP-7 around 15.2^{o}-35^{o}, were not observed for the other BINP polymers and the peaks were attributed to the periodicity parallel to the polymer chains[20, 23]. These very broad diffraction peaks indicated that the BINP-1 to BINP-5 polymers were amorphous whereas the polymers of BINP-6 and BINP-7 were crystalline.[24]

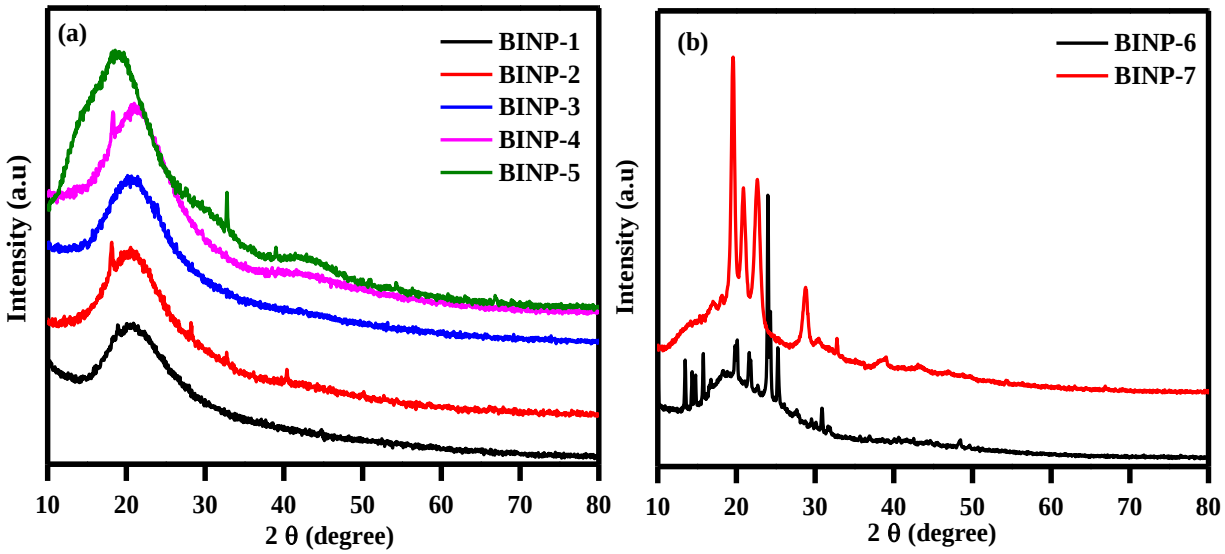

Figure 2. XRD-diffraction patterns of the synthesized BINP polymers. The broad peaks (a) indicated the polymers (BINP-1 to BINP-5) were amorphous, compared to (b) crystalline BINP-6 and BINP-7 with very sharp diffraction peaks.

Solid-state ^{13}C-NMR

The solid-state NMR spectra of BINP polymers except BINP-3 and BINP-4 (Figure 3a) displayed a broad peak around 110-150 ppm, a feature of the aromatic carbons in the BINP polymers (d, e, f, g, and h).[23–27] The peak "a" s at 40 ppm was assigned to the aliphatic carbon in the polymer ethyl chain. Concerning the peak corresponding to carbon singly-bound to nitrogen in the aliphatic chain, a peak "b" around 60-70 ppm represented carbon singly bound to nitrogen, and peak "c" around 158-162 ppm was attributed to aromatic carbonalkylated with nitrogen. The sharp peak at 162 ppm (BINP-3 and BINP-4) was denoted to the triazine ring [26] whereas the peak at 152 corresponded to the carbon singly bound to the oxygen atom. For BINP-3 and BINP-4, (Figure

3a), a broad peak "j" between 160-175 ppm was observed,[27] denoting the aromatic carbons bonded with nitrogen in the polymer chain. Moreover, only one broad peak was observed in BINP-3 and BINP-4 due to the equivalent protons, which were in the same environment and attached to the same atoms. For these two polymers, the environment for carbon is fewer than the member of symmetrical carbon atoms. The peak "i" around 45-65 ppm was designated to the aliphatic carbons in the chain. All the BINP polymer structures were provided in the Supporting Information. The broad peaks were initiated by large molecules with slow tumbling times relative to the time scale of NMR relaxation. Overall, these solid-state ^{13}C NMR spectra confirmed the formation of the seven polymers, five amorphous and two crystalline.

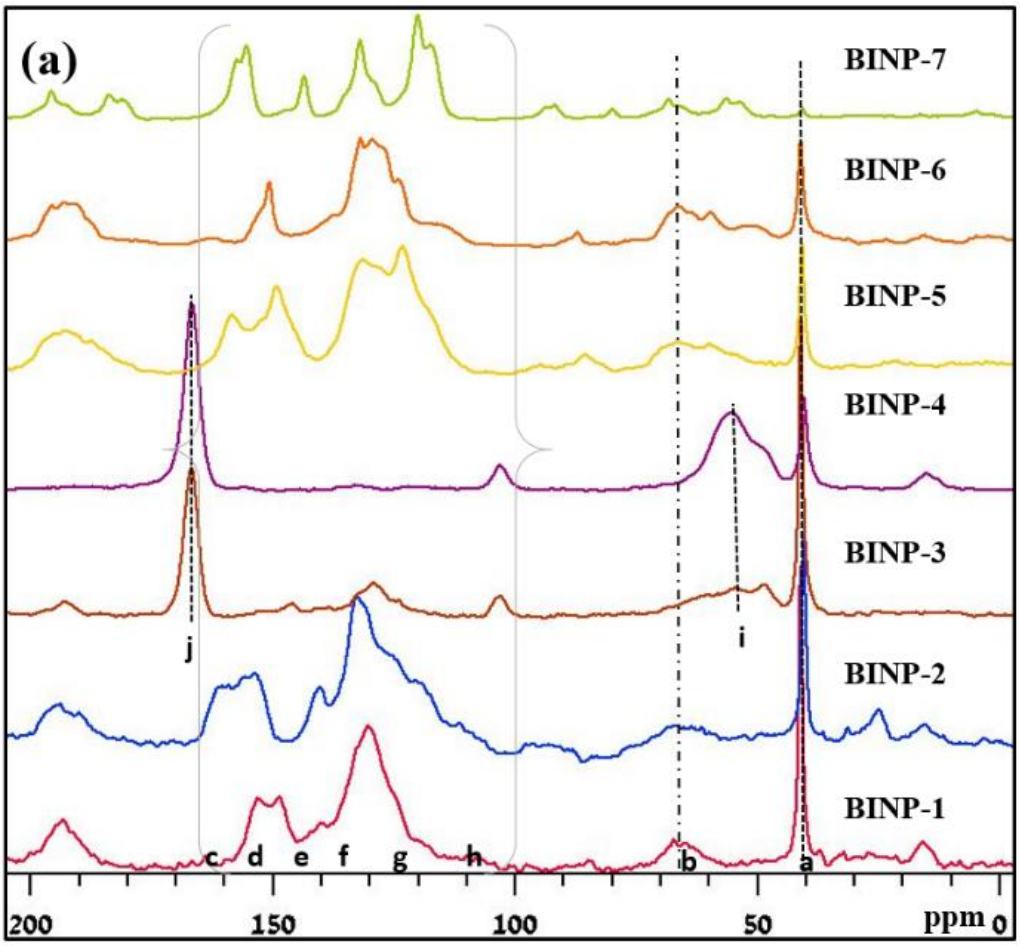

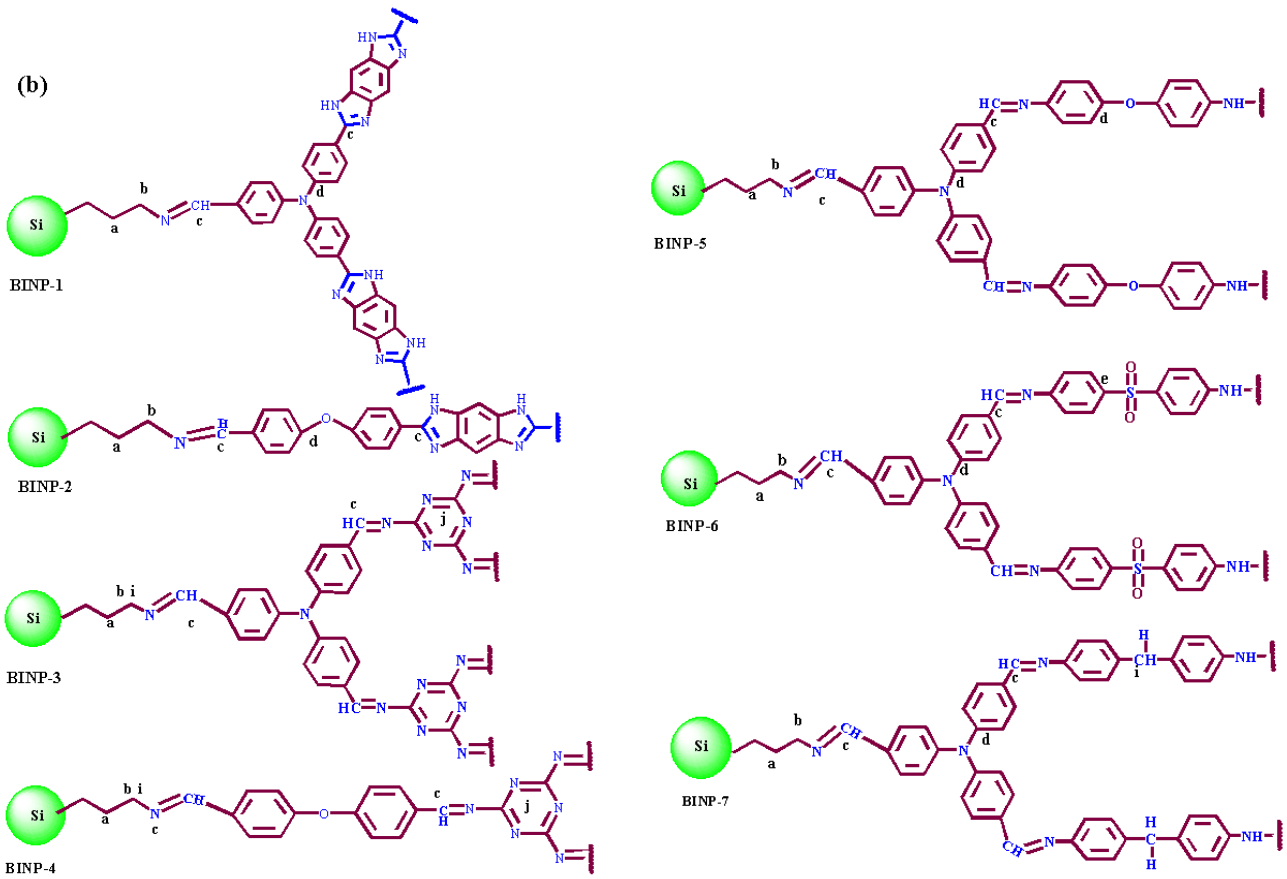

Figure 3. (a) Solid-state ^{13}C NMR spectra of all synthesized BINP polymers and (b) The chemical structures of the BINP polymers.

Morphology and dimension

SEM images and SEM-EDS basic elemental mapping of the benzimidazole polymers are shown in Figure 4a. The benzimidazole polymers exhibited irregular morphology with an average size of 4 µm. The EDX spectra and SEM-EDX elemental mapping spectra of the benzimidazole polymers displayed the elementary components (C, N, and Au) with uniform distribution. For SEM analysis, a small amount of the material was placed on a carbon tape attached to a copper strip, and the

benzimidazole polymers were coated with a thin layer of gold to enhance the polymer conductivity. The presence Si in the benzimidazole polymers was confirmed by SEM-EDS elemental mapping spectra. (Fig. 3b).

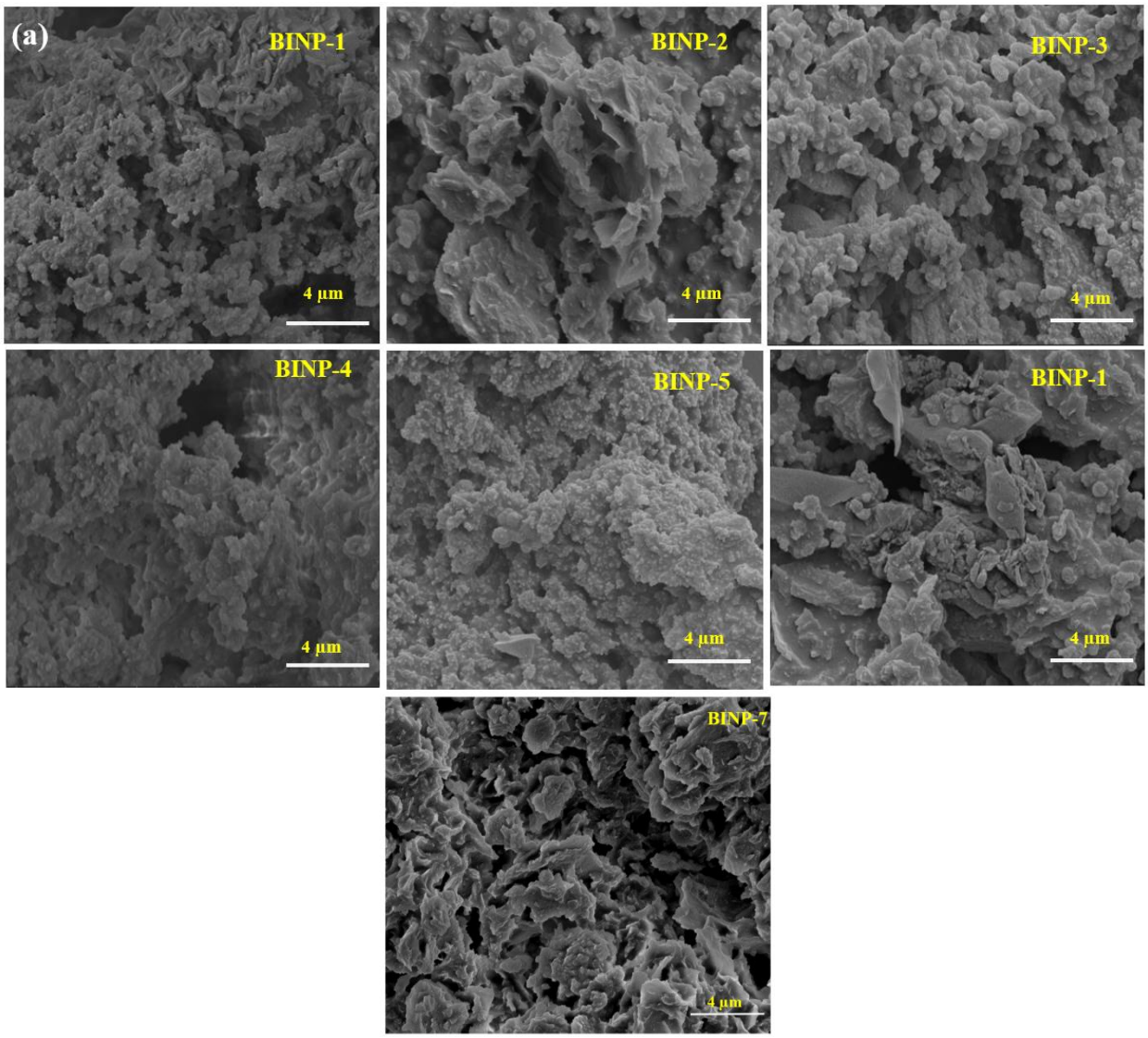

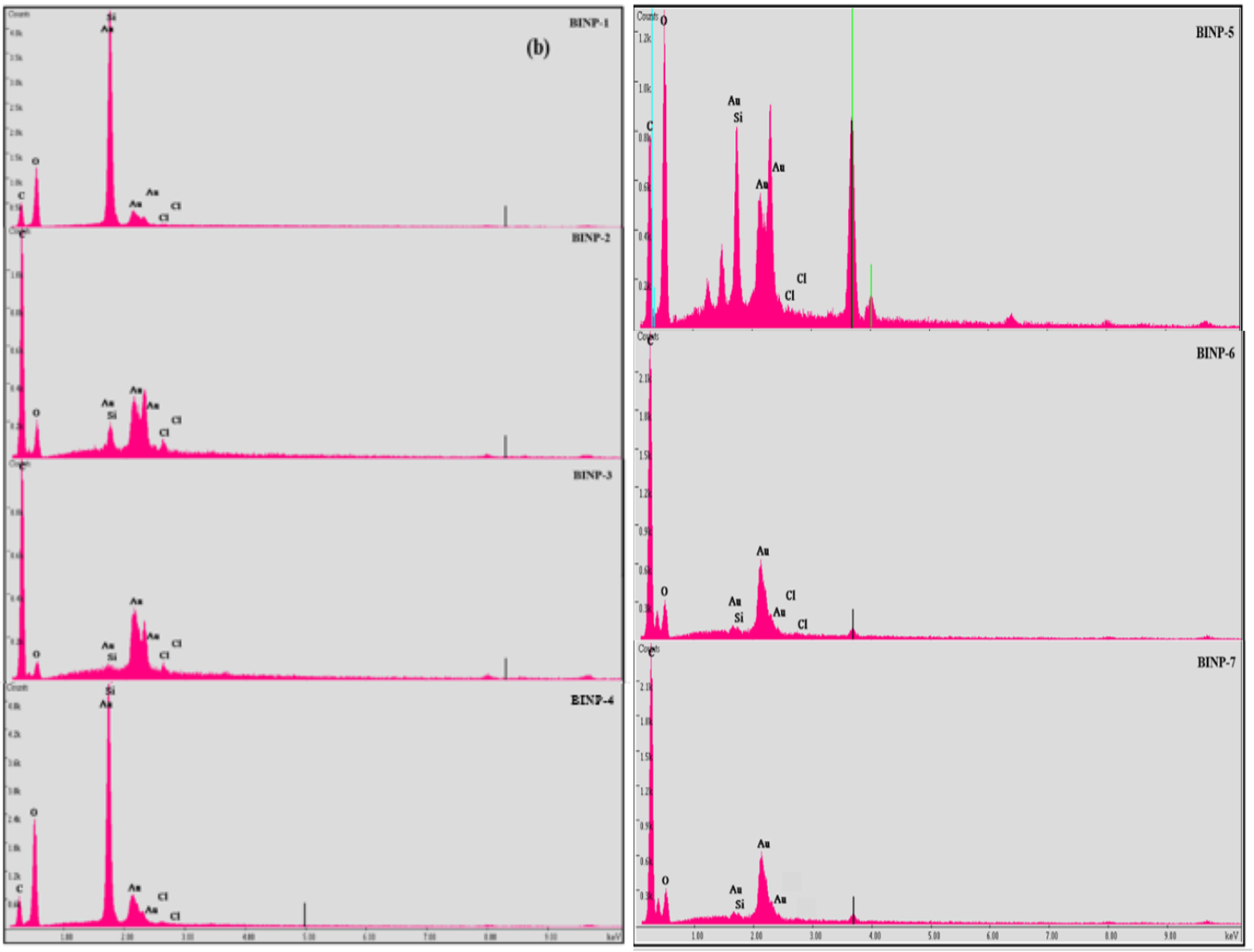

Figure 4. (a) SEM images of the BINP polymers, and (b) SEM-EDX of the BINP polymers.

Adsorption of CO_2

The CO_2 adsorption and desorption behavior of the polymers is shown in Figure 5. After the initial treatment step as described in the Experimental section, the BINP polymers were subjected to a flow of the CO_2 gas at room temperature for 80 min. The CO_2 adsorption onto the polymers was estimated by the weight increase of the materials upon their contact with CO_2. When the adsorption attained equilibrium, the CO_2 was switched back to the N_2 gas to initiate the desorption process

and this process was prolonged for 40 min. The desorption quantity of CO_2 was estimated from the polymer weight loss.

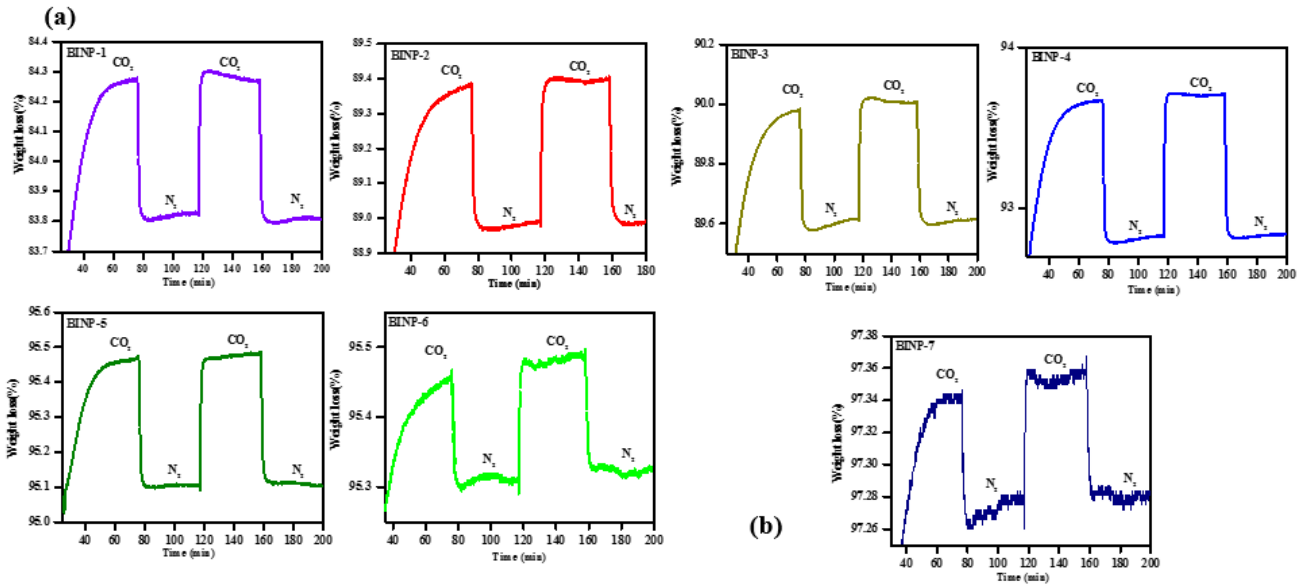

Figure 5. (a and b) Weight losses of the BINP polymers examined by TGA. The BINP polymers were exposed to a flow of N_2 at 25 ^{0}C for 40 min. then at 600 °C for 5 h. The system was then set back to 25 ^{0}C and the polymers were subjected to a flowing stream of CO_2 for 20 min (adsorption) and then switched to an N_2 stream for 20 min to invoke the desorption step.

All examined BINP polymers were treated by the same procedure for the adsorption with various CO_2 gas adsorption response on their surface, the CO_2 response for all the BINP polymers are shown in Figure 5 as a function of time. A gradual weight loss of the treated polymer was observed during the preliminary treatment of N_2 flow owing to the water and CO_2 desorption at ambient temperature. Such results illustrated the adsorption of CO_2 on the polymer surface whereas the weight loss signified the desorption of the CO_2 once the TGA system was switched back to the N_2 gas.

The CO_2 adsorption capacity

At first glance, the solid polymers must have adsorption capacities well above 3-4 mmol CO_2/g adsorbent (132-176 mg/g) to be competitive to the conventional scrubbing technology using monoethanolamine. However, the reusability, fast adsorption/desorption kinetics and the cost of adsorbents also play an important role to dictate the economic feasibility for large-scale operations. The CO_2 adsorption capacity of the BINP polymers was estimated from the TGA curves. The adsorption quantity of CO_2 for each BINP polymer as a function of time, Ads_{CO_2} (t), and the quantity of the CO_2 adsorption by per unit gram of the BINP polymers were calculated. In equations 1-2, m_s (t_0) is the initial mass of the BINP polymers before switching the CO_2 flow and $m_{CO2\text{-}ads}(t)$ is the mass of CO_2 adsorbed onto the BINP polymers as a function of time, [28]. The difference of the initial mass $m_s(t_0)$ of the polymer from its final mass represents the maximal amount of adsorbed CO_2 on the polymer.

$$m_{CO_2-ads} = m_s(t_0) - m_s(t_m) \quad (1)$$

$$Ads_{CO_2}(t) = {}^{100 * m_{CO_2-ads}}\Big/_{m_s(t_0)} \quad (2)$$

Thus, the adsorption capacity of CO_2 via the BINP polymers as a function of time $Ads_{CO_2}(t)$ was calculated as the ratio of the mass of carbon dioxide adsorbed by the BINP polymers over the mass at t_0 in equation 2. The maximum adsorption $Ads_{CO_2}(t)$ of the CO_2 and the CO_2 quantity adsorbed on the BINP polymer were provided in Figure S1 (Supporting Information). Moreover, nearly 20 min were required to reach the maximum adsorption (Ads_{CO_2} in mg CO_2/g of polymers) of CO_2 over the BINP polymers. This phenomenon was controlled through the thermodynamics of the CO_2-BINP polymers and the diffusion kinetics of CO_2 in the polymer matrix. Worth noting was a significant quantity of CO_2 that remained adsorbed on the polymer surface after a few hours of N_2

flow treatment at 25 ^{o}C. A broad range in the system could be due to the CO_2-BINP polymer interaction during the adsorption of CO_2 flow at 25 ^{o}C. Besides, some of CO_2 was desorbed spontaneously at 25 ^{o}C when the flow of CO_2 was stopped as the desorption was effectuated from the bridged carbonates and hydrogenocarbonates. However, the monodenate, bidentate and polydentate carbonates are required more than 600 ^{o}C to desorb from the polymer surface. As a result, there are two types of CO_2 interaction onto the BINP polymer to adsorb the maximum quantity of CO_2. The first interaction is the bridged carbonates and hydrogenocarbonates forms a weak interaction at 25 ^{o}C and desorbed by switched back to N_2 onto the BINP polymers. The second type, monodenate, bidentate and polydentate carbonates are forming a strong interaction with BINP polymer, it's impossible to desorb these carbonates at 25 ^{o}C. The adsorption of Ads_{max} and Ads_{strong} are plotted as a function of the adsorption quantity of CO_2 BINP polymer in Fig. S1 (Supporting Information).

Adsorption mechanism vs polymer physicochemical properties

There are two types of adsorption; physisorption and chemisorption, which are governed by the pore structure characteristics and the chemical structure of the sorbents, respectively. The BINP polymer was supported by functionalized silica for the suitable orientation of the polymer chain. The -NH of the polymers would form hydrogen bonding with the oxygen of CO_2 whereas the N atom of the five or six carbon ring exhibits interaction with the C atom of CO_2, known as tertrel bonds [29]. The nitrogen-enriched BINP and triazine based polymer show a better adsorption quantity of CO_2 with a minimum quantity of balance purge of 80 mL/min for the CO_2 capture. The triazine based polymers of BINP-3 and BINP-4 exhibited the maximum adsorption quantity of CO_2, compared to other BINP polymers. The better adsorption on BINP-3 and BINP-4 could be due to the triazine based chain and more nitrogen contents as well as the surface area of the

polymers. Apparently, such results were ascribed to N sites in the triazine rings, which facilitated the interaction with the polarizable CO_2 via the tetrel bonds as mentioned earlier. The triazine based polymers of BINP-4 and BINP-4 were adsorbed maximum amount of CO_2 on their surface as reflected by their highest content of nitrogen the capture of 13.2 and 7.7 mg/g, compared to 7.9 mg/g of BINP-1 (Fig. 6 b,c). In contrast, two crystalline polymers; BINP-6 and BINP-7 exhibited the lowest adsorption capacity for CO_2 and such results were corroborated with their lowest nitrogen contents (Table S2). There were minimal N atoms available for binding to CO_2 because they formed intermolecular hydrogen bonding with their adjacent O atoms of the SO_2 moiety. Furthermore, π-π interaction effectively prevented the polymer N sites to interact with polarized CO_2 molecules. BINP-7 has a lower pore size, compared to BINP-6. Thus, the adsorption capacity for CO_2 of BINP-7 (3.2 mg/g) with a surface area of 99 m^2/g was even lower than that of BINP-6 (4 mg/g) with a surface area of only 23 m^2/g). Similarly, BINP-5 with low pore sizes showed the minimum quantity of the CO_2 adsorption. BINP-1, BINP-2, and BINP-3 with large pores possessed the noticeable adsorption of CO_2. Such collective results illustrated that the binding of CO_2 was strongly dependent upon the participation of the N and N-H sites and the pore size of the polymer.

The high adsorption of CO_2 on the polymer is also due to the high specific surface area determined by adsorption of N_2 as shown in Figure 6d. The BET results are given in Table S1 (Supporting Information). The adsorption of CO_2 on the polymers corresponds to the following order BINP-4 > BINP-3 > BINP-1 > BINP-2, in corroboration with their specific surface area: 281, 108, 64, 32 m^2/g. The highest adsorption of CO_2 of BINP-4 was expected due to its highest surface area and the largest pores size (Table S1). From the N_2 adsorption-desorption isotherm presented in Fig. S2, the porous structure of BINP-4 corresponds to class II isotherm of H3 hysteresis loop (JUPAC

classification) typical for macrospores. The plot of adsorbed CO_2 vs pore size was linear with an acceptable correlation coefficient (R^2 = 0.892), signifying the role of the pore size in the adsorption of CO_2 (Supporting Information Figure S3).

.

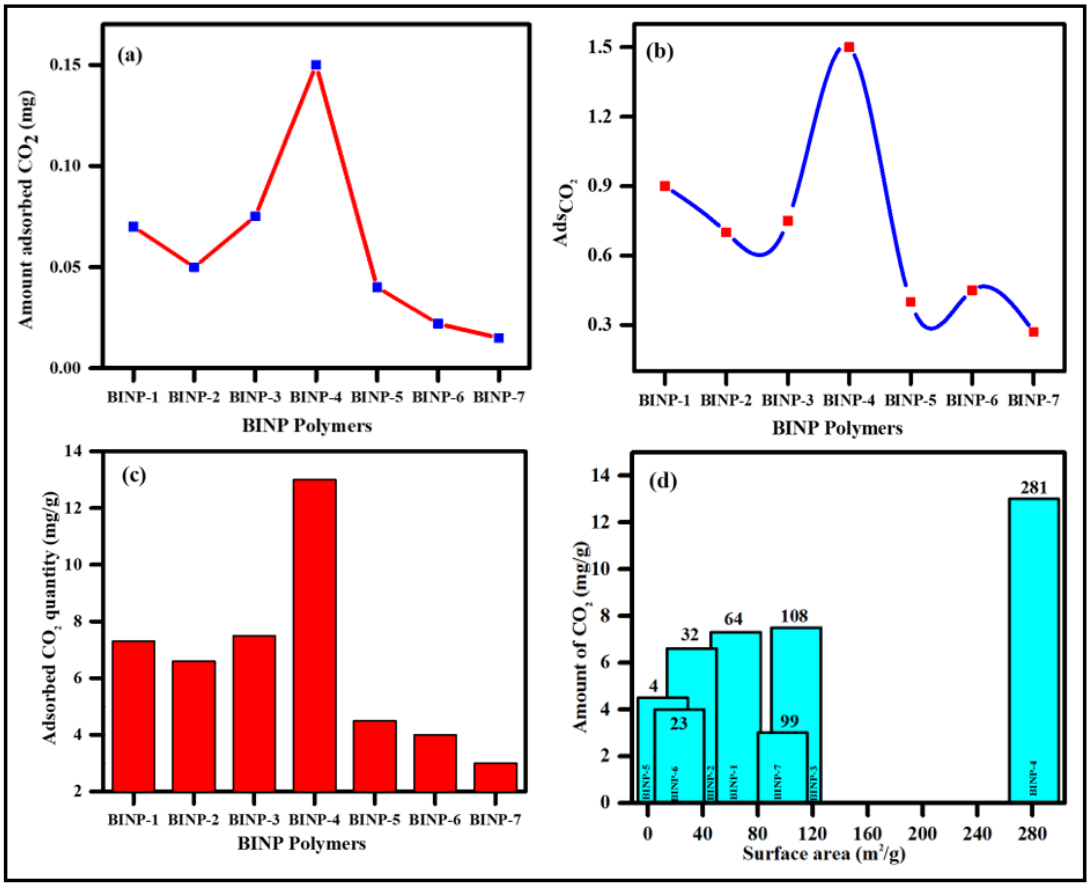

Figure 6. (a) The adsorption of CO_2 onto the BINP polymers, (b) The adsorption of CO_2 (mg) estimated from equation 2, (c) the adsorption quantity of CO_2 per unit gram of the BINP polymers and (d) The adsorption amount of CO_2 vs the surface area of the BINP polymers by BET.

The operating temperature would be anticipated to play an important role in the CO_2 adsorption/desorption process. However, this option was not attempted here to avoid the use of extra energy. To date, inorganic materials have been extensively used for CO_2 adsorption/desorption processes such as CeO_2 nanopowders, [30] PEI+TEPA, [31] $CaO/CaCO_3$, [5]

copper hexacynanoferrate, [11] and solvothermal synthesized CeO_2 nanopowders. [9] However, these materials are expensive and the adsorption process requires a high amount of gas flow (200 mL/min) and involves a large quantity of these adsorbents.

Conclusion

The silica-supported polymers were synthesized and investigated for the studies of the CO_2 adsorption by thermogravimetric analysis. The surface area, pore size as well as the nitrogen enrichment of the polymers, revealed the efficient adsorption capacity of CO_2 over the polymer surface. The adsorption of CO_2 gas onto the BINP polymers was partially reversible at room temperature and providing the quantification of the BINP-CO_2 types that was desorbed by switching the N_2 gas and CO_2 leftover on the polymer surface of. The BINP polymers were regenerated for repeated adsorption/desorption of CO_2 without diminishing their performance properties. Work is in progress to investigate high pressure gas uptake towards the improvement of CO_2 adsorption capacity considering the quantity of gas uptake is highly dependent on the gas pressure [32].

Associated content

Supporting Information

Detailed information to show the maximum adsorption capacity of CO_2 onto the polymers, BET results of the polymers, a linear plot of the pore size vs the adsorption amount of CO_2 onto the BINP polymers, and the XPS spectra of the polymers.

Notes

The authors declare no competing financial interest.

References

(1) Neti, P. S. V. K.; Wu. X.; Peng. P.; Deng, S. Synthesis of a benzothiazole nanoporous polymer for selective CO_2 adsorption. *RSC Adv.* **2014**, 1, 9669–9672.

(2) Neti, V. S. P. K.; Wang, J.; Echegoyen, L. Selective CO_2 adsorption in a porphyrin polymer with benzimidazole linkages. *RSC Adv.* **2015**, 5, 10960–10963.

(3) Sekizkardes, A. K.; Altarawneh, S.; Kahveci, Z.; Timur, I.; El-Kaderi, H. M. Highly selective CO_2 capture by triazine-based benzimidazole- linked polymers. *Macromolecules,* **2014**, 47, 8328−8334.

(4) Bhunia, S.; Bhanja, P.; Das, S. K.; Sen, T.; Bhaumik, A. Triazine containing N-rich microporous organic polymers for CO_2 capture. *J. Solid State Chem.,* **2017**, 247, 113–119.

(5) Santos, E. T.; Alfonsín, C.; Chambel, A. J. S.; Fernandes, A.; Dias, A. P. S.; Pinheiro, C. I. C.; Ribeiro, M. F. Investigation of a stable synthetic sol-gel CaO sorbent for CO_2 capture. *Fuel*, **2012**, 94, 624–628.

(6) Rehman, A.; Park, S. Facile synthesis of nitrogen-enriched microporous carbons derived from imine and benzimidazole-linked polymeric framework for efficient CO_2 adsorption. *J. CO_2 Util.*, **2017**, 21, 503–512.

(7) Ravi, S.; Puthiaraj, P.; Ahn, W. Cyclic carbonate synthesis from CO_2 and epoxides over diamine- functionalized porous organic frameworks. *J. CO_2. Util.*, **2017**, 21, 450–458.

(8) Das, S. K.; Wang, X.; Lai, Z. Facile synthesis of triazine-triphenylamine-based microporous covalent polymer adsorbent for flue gas CO_2 capture. *Microporous Mesoporous Mater.*, **2018**, 255, 76–83.

(9) Slostowski, C.; Marre, S.; Dagault, P.; Babot, O.; Toupance, T.; Aymonier, C. CeO2 nanopowders as solid sorbents for efficient CO2 capture/release processes. *J. CO_2. Util.,* **2017**, 20, 52–58.

(10) Liu, F.; Huang, K.; Yoo, C.; Okonkwo, C.; Tao, D.; Jones, C. W. Facilely synthesized meso-macroporous polymer as support of poly (ethyleneimine) for highly efficient and selective capture of CO_2. *Chem. Eng. J.*, **2017**, 314, 466–476.

(11) Ojwang, D. O.; Grins, J.; Svensson, G. The adsorption kinetics of CO_2 on copper hexacyanoferrate studied by thermogravimetric analysis. *Microporous Mesoporous Mater.*, **2018**, 272, 70–78.

(12) Li, H.; Ding, X.; Zhao, Y.; Han, B. Preparation of mannitol-based ketal-linked porous organic polymers and their application for selective capture of carbon dioxide. *Polymer*, **2016**, 89, 112–118.

(13) Yan-Chao Zhao, B. H. H.; Qian-Yi. Zhou, D.; Wang, T. Preparation and characterization of triptycene-based microporous poly (benzimidazole) networks. *J. Mater. Chem.*, **2012**, 22, 11509–11514.

(14) Zul, S. I.; Sarwar, Yavuz, C. T. Melamine based porous organic amide polymers for CO_2 capture. *RSC. Adv.*, **2014**, 4, 52263–52269.

(15) Hu, X.; Chen, Q.; Sui, Z.; Zhao, Bovet, Z., Laursen, N. B. W.; Han, B. Triazatriangulenium-based porous organic polymers for carbon dioxide capture. *RSC. Adv.*, **2015**, 5, 90135–90143.

(16) Rabbani, M. G.; Reich, T. E.; Kassab, R. M.; Jackson, K. T.; El-Kaderi, H. M. High CO_2 uptake and selectivity by triptycene-derived benzimidazole-linked polymers. *Chem. Comm.*, **2012**, 48, 1141–1143.

(17) He, Y.; Xu, T.; Hu, J.; Peng, C.; Yang, Q.; Wang, H.; Liu, H. Amine functionalized 3D porous organic polymer as an effective adsorbent for removing organic dyes and solvents. *RSC. Adv.*, **2017**, 7, 30500–30505.

(18) Xu, X.; Wood, C. D. A Highly Tunable approach to enhance CO_2 capture with liquid llkali/amines. *Env. Sci. Technol.*, **2018**, 52, 10874-10882.

(19) Meconi, G. M.; Tomovska, R.; Zangi, R. Adsorption of CO_2 gas on graphene–polymer composites. *J. CO_2. Util.*,, **2019**, 32, 92-105.

(20) Maruthapandi, M.; Kumar, V.B.; Levine, M.; Gedanken, A. Fabrication of poly (4,4′-oxybisbenzenamine) and its conjugated copolymers initiated by easily accessible carbon dots. *Eur. Polym. J.*, **2018**, 109, 153–161.

(21) Maruthapandi, M.; Gedanken, A.; A short report on the polymerization of pyrrole and its copolymers by sonochemical synthesis of fluorescent carbon dots. *Polymers*, **2019**, 11, 1240.

(22) Maruthapandi, M.; Luong, J. H. T.; Gedanken, A. Kinetic, isotherm and mechanism studies of organic dye adsorption on poly(4,40- oxybisbenzenamine) and copolymer of poly(4,40-oxybisbenzenamine-pyrrole) macro-nanoparticles synthesized by multifunctional carbon dots. *New J. Chem.*, **2019**, 43, 1926–1935.

(23) Maruthapandi, M.; Kumar, V. B.; Porat, Z.; Gedanken, A. Novel polymerization of aniline and pyrrole by carbon dots. *New J. Chem.*, **2018**, 42, 535–540.

(24) Ranjeesh, K. C.; Illathvalappil, R. S.; Veer, D.; Kurungot, S.; Babu, S. S. Imidazole-linked crystalline two-dimensional polymer with ultrahigh proton-conductivity. *J. Am. Chem. Soc.*, **2019**, 141, 14950–14954.

(25) Maruthapandi, M.; Nagvenkar, A. P.; Perelshtein, I.; Gedanken, A. Carbon-dot initiated synthesis of polypyrrole and polypyrrole@CuO micro/nanoparticles with enhanced antibacterial activity. *ACS Appl. Polym. Mater.* **2019**, 1, 1181–1186.

(26) Lv, Z.; Zhao, D.; Xu. S. Facile synthesis of mesoporous melamine formaldehyde spheres for carbon dioxide capture. *RSC Adv.*, **2016**, 6, 59619–59623.

(27) Young, C.; Yamauchi, Y.; Kuo, S. Strategic design of triphenylamine- and triphenyltriazine-based two-dimensional covalent organic frameworks for CO_2 uptake and energy storage. *J. Mater. Chem. A.*, **2018**, 6, 19532–19541.

(28) Maruthapandi, M.; Eswaran, L.; Luong, J. H. T.; Gedanken, A. Sonochemical preparation of polyaniline @ TiO_2 and polyaniline@ SiO_2 for the removal of anionic and cationic dyes. *Ultrason. Sonochem.*, **2019**, 104864.

(29) Del Bene, J. E.; Elguero, J.; Alkorta, I. Complexes of CO2 with the azoles: tetrel bonds, hydrogen bonds and other secondary interactions. *Molecules*, **2018**, 23, 906.

(30) Li, M.; Tumuluri, U.; Wu, Z.; Dai, S. Effect of dopants on the adsorption of carbon dioxide on ceria surfaces. *Chem. Sus. Chem*., **2015**, 8, 3651–3660.

(31) Chen, C.; Yang, S.; Ahn, W.; Ryoo, R. Amine-impregnated silica monolith with a hierarchical pore structure : enhancement of CO_2 capture capacity. *Chem. Comm.*, **2009**, 24, 3627–3629.

(32) Rabbani, M. G.; El-Kaderi, H. M. Synthesis and characterization of porous benzimidazole-linked polymers and their performance in small gas storage and selective uptake. *Chem. Mater*., **2012**, 24, 1511−1517.